Available online at www.sciencedirect.com
ScienceDirect
Ceramics International 36 (2010) 1993–1996
CERAMICS INTERNATIONAL
www.elsevier.com/locate/ceramint

Short communication

Preparation of nickel ferrite from thermolysis of nickel tris(malonato)ferrate(III) heptahydrate precursor

B.S. Randhawa [a,*], Jashanpreet Singh [a], Harpreet Kaur [a], Manpreet Kaur [b]

[a] Department of Chemistry, Guru Nanak Dev University, Amritsar 143005, India
[b] Lyallpur Khalsa College, Jalandhar 144001, India

Received 27 January 2010; received in revised form 14 February 2010; accepted 18 March 2010
Available online 27 April 2010

Abstract

The thermal decomposition of nickel tris(malonato)ferrate(III) heptahydrate precursor, $Ni_3[Fe(CH_2C_2O_4)_3]_2{\cdot}7H_2O$ has been investigated from ambient temperature to 1073 K in static air atmosphere using various physico-chemical techniques, i.e. TG–DTG–DSC, XRD, Mossbauer and IR spectroscopy. The precursor undergoes dehydration and decomposition simultaneously to yield nickel malonate and iron(II)malonate intermediates at 513 K. At higher temperature (593 K) these intermediate species decompose to NiO and α-Fe_2O_3, respectively. Finally, nickel ferrite, $NiFe_2O_4$ has been obtained as a result of solid-state reaction between Fe_2O_3 and NiO at a temperature (673 K) much lower than that of the conventional ceramic method. SEM analysis of the final thermolysis product reveals the formation of nickel ferrite nanoparticles with an average particle size of 40 nm. Magnetic studies show that these particles possess a saturation magnetization and Curie temperature of 2970 G and 843 K, respectively. Lower magnitude of these parameters as compared to the bulk values may be attributed to the ultrafine nature of the ferrite particles.

Keywords: A. Calcination; B. Thermal analysis; C. X-ray method; D. Mössbauer spectroscopy; E. Ferrites

1. Introduction

Although the most extensively used technique for the bulk preparation of ferrites is the conventional ceramic method, it has certain limitations viz. (i) milling of the starting materials which incorporates lattice defects and strains in the ferrite obtained, thus affecting its permanent magnetic properties and (ii) sintering at high temperature for a long time results in particle coarsening and aggregation, i.e. loss of the fine particle nature. Thus, this technique cannot be used for the preparation of nanosized ferrites. On the other hand, the precursor method does not involve any milling of the starting materials and there is direct mixing of the cations on atomic scale. Moreover, the exothermic decomposition of the precursor provides heat to the solid-state reaction, thus decreasing the external temperature required for the obtention of ferrites. Therefore, ferrites can be formed at lower temperature and in shorter time. Evolution of gaseous products during decomposition of the precursor dissipates the heat and prevents sintering, thereby leading to the formation of stoichiometrically pure and single-phase nanosized ferrites with large surface area. The present investigation deals with the preparation of nickel ferrite ($NiFe_2O_4$) by precursor method. $NiFe_2O_4$ finds an extensive application in ferrofluids, magnetic fluids, magnetic recording media, magnetic resonance imaging, transformer/electromagnetic cores, electronic devices, catalysis, magnetic refrigeration systems and gas sensors [1–9]. It has also become a potential material in electrochemistry because of its application as inert anode in aluminium electrolysis [10–13].

2. Experimental procedure

Nickel tris(malonato)ferrate(III) heptahydrate, $Ni_3[Fe(CH_2C_2O_4)_3]_2{\cdot}7H_2O$ precursor prepared by mixing stoichiometric quantities of aqueous solutions of ferric malonate, malonic acid and nickel carbonate. The reaction mixture was stirred vigorously at 373 K till a clear solution was obtained. It was then concentrated on water bath and the precipitates of nickel ferrimalonate precursor were obtained by adding excess of ethanol to it. The precursor was air-dried and stored in vacuum desiccator. The identity of the precursor was established by

* Corresponding author.
E-mail address: balwinderrandhawa@yahoo.co.in (B.S. Randhawa).

0272-8842/$36.00
doi:10.1016/j.ceramint.2010.03.034

elemental analysis: [(C, % = 20.83 (obsd.), 21.03 (calc.); H% = 2.50 (obsd.), 2.53 (calc.); Fe% = 10.71 (obsd.), 10.91 (calc.); Ni% = 17.18 (obsd.), 17.23(calc.)].

Simultaneous TG–DTG–DSC curves were recorded on a Pyris Diamond Model (Perkin-Elmer) at a heating rate of 10 K min^{-1} in flowing air atmosphere from ambient to 1073 K. The experimental details for recording IR, Mössbauer, XRD Powder, SEM and Magnetic data are reported elsewhere [14–16]. For the identification of intermediates and products, the precursor was also calcined isothermally in silica crucible. The variation in temperature was kept ±5 K during isothermal calcinations.

3. Results and discussion

IR spectrum of nickel tris(malonato)ferrate(III) heptahydrate precursor shows a broad band centered around 3370 cm^{-1} due to ν(O–H) of lattice water. A shoulder at 2900 cm^{-1} is assigned to ν(C–H) of the malonate ligand. A broad band centered at 1580 cm^{-1} attributes to ν_{asym}(C=O) while bands in the range 1370–1450 cm^{-1} are associated with ν_{sym}(C=O). Some small but distinct bands in the range 950–1200 cm^{-1} are assigned to ν(C–O), ν(C–C) and (O–H) bending modes. The bands at 575 and 440 cm^{-1} suggest the presence of Fe–O (carboxylate) bonding [17,18]. Mössbauer spectrum of the precursor exhibits a doublet (Fig. 1) with isomer shift (δ) and quadrupole splitting (Δ) values of 0.37 and 0.49 mm s^{-1}, respectively. These parameters agree with those reported for the high spin Fe(III) complexes showing octahedral geometry [19]. The coordination number 6 for iron is satisfied by three malonate ligands that bind to iron through oxygen atoms of the carboxylate groups. The transition metal ion and water molecules seem to be responsible for linking together the complex ion, $[Fe(mal)_3]^{3-}$.

Simultaneous TG–DTG–DSC curve of nickel tris(malonato)ferrate(III) heptahydrate precursor are displayed in Fig. 2. The dehydration of the precursor is immediately followed by decomposition till a mass loss of 25% is attained at 513 K indicating the formation of iron(II)malonate and nickel malonate intermediates. These two endothermic steps are clearly visible in DTG and DSC with ΔH values of 174.6 and 351.9 kJ mol^{-1}, respectively. The existence of iron(II)malonate has been confirmed by recording Mössbauer parameters of the residue (Table 1) obtained by isothermal calcination of the precursor at 523 K for 15 min. The intermediates undergo an abrupt oxidative pyrolysis till a mass loss of 62.3% is reached at 593 K suggesting the formation of oxide phases, i.e. NiO and Fe_2O_3. This process is accompanied by a strong exotherm with $\Delta H = -2171.1$ kJ mol^{-1}. Mössbauer spectrum (Fig. 3) of the residue obtained by calcining the precursor at 593 K for 15 min exhibits three overlapping sextets and a central doublet. The Mössbauer parameters (Table 1) confirm the presence of a mixture of unreacted α-Fe_2O_3 and $NiFe_2O_4$ while XRD powder pattern (Fig. 4) displays signals due to α-Fe_2O_3, NiO and

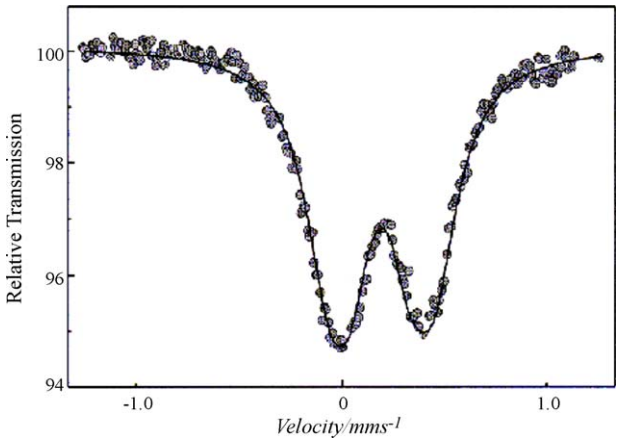

Fig. 1. Mössbauer spectrum of nickel tris(malanato)ferrate(III) heptahydrate precursor at 298 K.

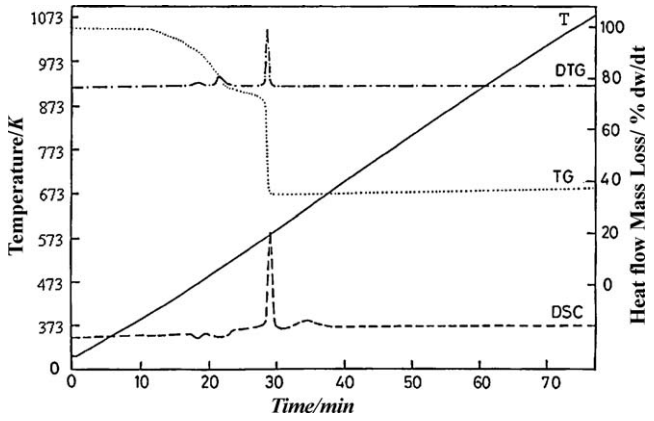

Fig. 2. Simultaneous TG–DTG–DSC curves of nickel tris(malonato)ferrate(III) heptahydrate precursor.

Table 1
Mössbauer parameters of the thermolysis products of $Ni_3[Fe(mal)_3]_2 \cdot 7H_2O$ precursor recorded at 77 K.

Calcining temperature (K)	δ[a] (mm s^{-1})	Δ (mms^{-1})	B (T)	Fe^{3+} distribution	Assignment
513	1.38	1.80	–	–	$Fe^{II}CH_2C_2O_4$
593	0.48	0.02	54.2(S)	22%	α-Fe_2O_3
	0.48	–	50.4(S)	40%(oct)	$NiFe_2O_4$
	0.39	–	44.8(S)	26%(tet)	
	0.34	1.01	CD	12%	
673	0.47	–	52.8	28%(oct)	$NiFe_2O_4$
	0.38	–	49.1	72%(tet)	

[a] w.r.t pure iron absorber; CD, central doublet; S, Sextet; B, internal magnetic field in Tesla; oct, octahedral site; tet, tetrahedral site.

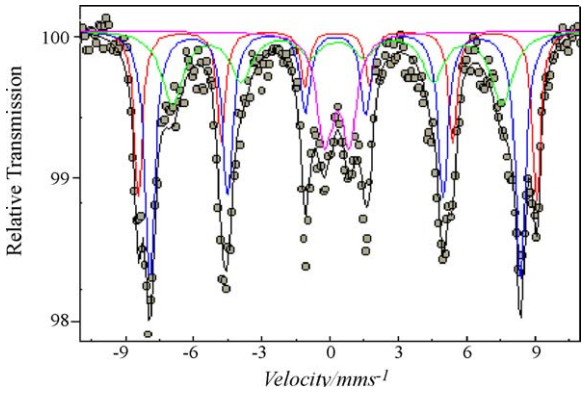

Fig. 3. Mössbauer spectrum of the residue obtained by calcining the precursor at 593 K for 15 min.

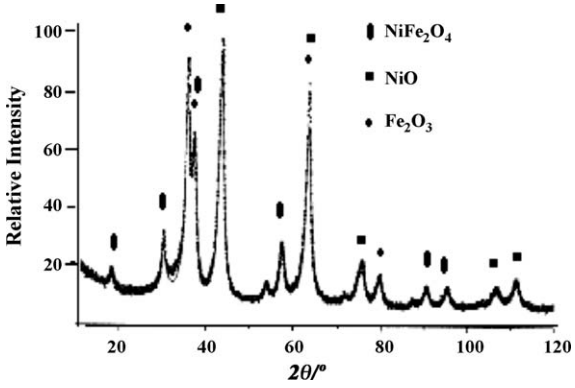

Fig. 4. XRD powder pattern of the residue obtained by calcining the precursor at 593 K for 15 min.

$NiFe_2O_4$. At higher temperature, a solid-state reaction between α-Fe_2O_3 and NiO continues as supported by an exothermic region in DSC in the temperature range 613–663 K ($\Delta H = -513.5$ kJ mol^{-1}). Mössbauer spectrum of the final thermolysis residue (Fig. 5) displays two overlapping sextets, the parameters (Table 1) of which agree with those reported for nickel ferrite, $NiFe_2O_4$. Formation of nickel ferrite has been further confirmed by XRD powder pattern (Fig. 6) of the final

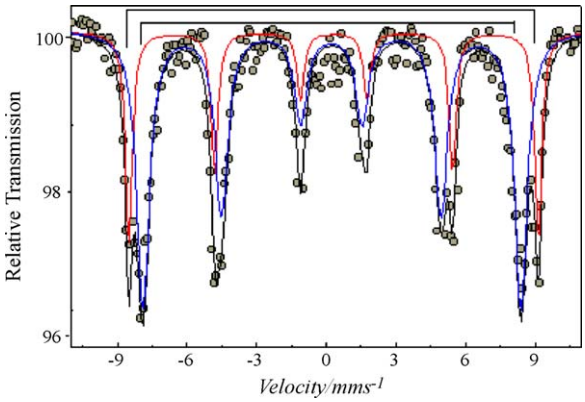

Fig. 5. Mössbauer spectrum of the final thermolysis residue.

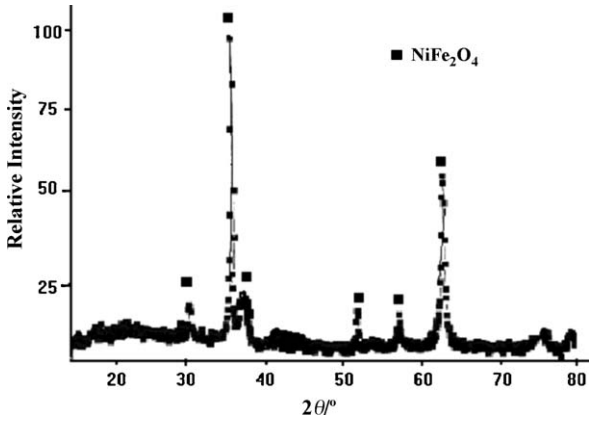

Fig. 6. XRD powder pattern of the final thermolysis residue.

thermolysis product after treating it with 2N HNO_3 to remove undesired NiO [20]. The ferrite obtained, i.e. $NiFe_2O_4$ has an average particle size of 40 nm as revealed by SEM analysis (Fig. 7).

Based on the above results, the following mechanism for the thermal decomposition of nickel tris(malonato)ferrate(III) heptahydrate precursor is proposed:

$$Ni_3[Fe(CH_2C_2O_4)_3]_2 \cdot 7H_2O \xrightarrow{513\,K} 3NiCH_2C_2O_4 + 2Fe^{II}CH_2C_2O_4 + \text{gaseous products}$$

$$3NiCH_2C_2O_4 + 2FeCH_2C_2O_4 \xrightarrow{593\,K} \frac{5}{2}NiO + \frac{1}{2}\alpha - Fe_2O_3 + \frac{1}{2}NiFe_2O_4 + \text{gaseous products}$$

$$\frac{5}{2}NiO + \alpha\text{-}Fe_2O_3 \xrightarrow{673\,K} NiFe_2O_4 + \frac{3}{2}NiO$$

In order to get pure ferrite, i.e. $NiFe_2O_4$, the final residue was treated with 2N HNO_3 to remove NiO.

Magnetic properties, i.e. saturation magnetization, Curie temperature, etc. possessed by the ferrites play a key role in establishing their supremacy over the metallic magnetic materials which cannot be used at microwave frequencies. Various magnetic properties of nickel ferrite obtained are listed

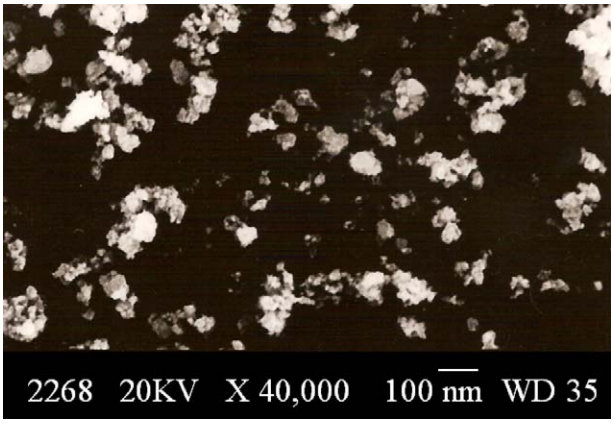

Fig. 7. SEM micrograph of the final thermolysis product.

Table 2
Magnetic parameters of $NiFe_2O_4$.

	Density (g cm^{-3})	Saturation magnetization (G)	Specific magnetization (G cm^{-3})	Curie temperature T_c (K)	Average grain size (nm)
$NiFe_2O_4$	4.52	2970	657	843	40

in Table 2. Since saturation magnetization and Curie temperature are particle size dependent, a decrease in particle size lowers the magnitude of these magnetic parameters [21].

References

[1] T. Pananparayil, R. Marande, S. Komameni, S.G. Sankar, A novel low-temperature preparation of several ferrimagnetic spinels and their magnetic and Mössbauer characterization, J. Appl. Phys. 64 (1988) 5641–5643.

[2] F.X. Redl, C.T. Black, G.C. Papaefthymiou, R.L. Sandstrom, M. Yin, H. Zeng, C.B. Murray, S.P. O'Brien, Magnetic, electronic, and structural characterization of nonstoichiometric iron oxides at the nanoscale, J. Am. Chem. Soc. 126 (2004) 14583–14599.

[3] S. Prasad, N.S. Gajbhiye, Magnetic studies of nanosized nickel ferrite particles synthesized by the citrate precursor technique, J. Alloys Compd. 265 (1998) 87–92.

[4] B.H. Sohn, R.E. Cohen, G.C. Papaefthymiou, Magnetic properties of iron oxide nanoclusters within microdomains of block copolymers, J. Magn. Magn. Mater. 182 (1998) 216–224.

[5] R.H. Kodama, Magnetic nanoparticles, J. Magn. Magn. Mater. 200 (1999) 359–372.

[6] F.D. Monte, M.P. Morales, D. Levy, A. Fernandez, M. Ocana, A. Roig, E. Molins, K. O'Grady, C.J. Serna, Formation of γ-Fe_2O_3 isolated nanoparticles in a silica matrix, Langmuir 13 (1997) 3627–3634.

[7] C. Castro, J. Ramos, A. Millan, J.G. Calbele, F. Palacio, Production of magnetic nanoparticles in imine polymer matrixes, Chem. Mater. 12 (2000) 3681–3688.

[8] K.S. Martirosyan, D. Luss, Carbon combustion synthesis of ferrites: synthesis and characterization, Ind. Eng. Chem. Res. 46 (2007) 1492–1499.

[9] B. Vishwanathan, V.R.K. Murthy, Ferrite Materials: Science and Technology, Springer-Verlag, 1990.

[10] J.D. Weyand, D.H. DeYoung, S.P. Ray, G.P. Tarcy, F.W. Baker, Inert Anode Aluminium Smelting, Final Report, Aluminium Company of America, vol. 16, Alcoa Laboratories, Alcoa Center, 1986 970 p..

[11] E. Olsen, J. Thonstad, Nickel ferrite as inert anodes in aluminium electrolysis. Part I. Material fabrication and preliminary testing, J. Appl. Electrochem. 29 (1999) 293–297.

[12] C.F. Windisch, An electrochemical impedance study on cermet anodes in alumina-saturated molten cryolite, J. Electrochem. Soc. 138 (1991) 2027–2029.

[13] E. Olsen, J. Thonstad, Nickel ferrite as inert anodes in aluminium electrolysis. Part II. Material performance and long-term testing, J. Electrochem. Soc. 29 (1999) 301–311.

[14] B.S. Randhawa, K. Gandotra, Synthesis of sodium ferrite by precursor and combustion methods: a comparative study, Ceram. Int. 35 (2009) 157–161.

[15] B.S. Randhawa, M. Kaur, A comparative study on the thermal decomposition of some transition metal maleates and fumarates, J. Therm. Anal. Calorim. 89 (2007) 251–255.

[16] B.S. Randhawa, H.S. Dosanjh, M. Kaur, Preparation of spinel ferrites from citrate precursor route: a comparative study, Ceram. Int. 35 (2009) 1045–1049.

[17] K. Nakamoto, Infrared Spectra of Inorganic and Coordination Compounds, 2nd ed., John Wiley Interscience, New York, 1978.

[18] C.N.R. Rao, Chemical Applications of Infrared Spectroscopy, Academic Press, New York, 1963.

[19] A. Vertes, L. Korecz, K. Burger, Mössbauer Spectroscopy, Elsevier Sci. Publ. Co., New York, 1979.

[20] ASTM Card No. 10-325.

[21] N.S. Gajbhiye, A. Vijayalakshmi, Synthesis of ultrafine $SrFe_{12}O_{19}$ particles with high coercivity, J. Phys. (France) 7 (1997) 329–330.